PCCP

PAPER

View Article Online
View Journal | View Issue



Cite this: *Phys. Chem. Chem. Phys.*, 2017, **19**, 8854

# Controlling adsorption and passivation properties of bovine serum albumin on silica surfaces by ionic strength modulation and cross-linking

Jae Hyeon Park,†[ab] Tun Naw Sut,†[ab] Joshua A. Jackman,[ab] Abdul Rahim Ferhan,[ab] Bo Kyeong Yoon[ab] and Nam-Joon Cho*[abc]

Received 28th February 2017,
Accepted 3rd March 2017

DOI: 10.1039/c7cp01310h

rsc.li/pccp

Understanding the physicochemical factors that influence protein adsorption onto solid supports holds wide relevance for fundamental insights into protein structure and function as well as for applications such as surface passivation. Ionic strength is a key parameter that influences protein adsorption, although how its modulation might be utilized to prepare well-coated protein adlayers remains to be explored. Herein, we investigated how ionic strength can be utilized to control the adsorption and passivation properties of bovine serum albumin (BSA) on silica surfaces. As protein stability in solution can influence adsorption kinetics, the size distribution and secondary structure of proteins in solution were first characterized by dynamic light scattering (DLS), nanoparticle tracking analysis (NTA), and circular dichroism (CD) spectroscopy. A non-monotonic correlation between ionic strength and protein aggregation was observed and attributed to colloidal agglomeration, while the primarily α-helical character of the protein in solution was maintained in all cases. Quartz crystal microbalance-dissipation (QCM-D) experiments were then conducted in order to track protein adsorption onto silica surfaces as a function of ionic strength, and the measurement responses indicated that total protein uptake at saturation coverage is lower with increasing ionic strength. In turn, the QCM-D data and the corresponding Voigt–Voinova model analysis support that the surface area per bound protein molecule is greater with increasing ionic strength. While higher protein uptake under lower ionic strengths by itself did not result in greater surface passivation under subsequent physiologically relevant conditions, the treatment of adsorbed protein layers with a gluteraldehyde cross-linking agent stabilized the bound protein in this case and significantly improved surface passivation. Collectively, our findings demonstrate that ionic strength modulation influences BSA adsorption uptake on account of protein spreading and can be utilized in conjunction with covalent cross-linking strategies to prepare well-coated protein adlayers for improved surface passivation.

## Introduction

The nonspecific adsorption of proteins on solid supports attracts wide attention due to its relevance for fundamental understanding of biological mechanisms (*e.g.*, clotting, immune recognition) and industrial processes (*e.g.*, surface passivation, fouling, hemoadsorption).[1–9] Experimentally, the mechanistic stages of protein adsorption have long been scrutinized, and the evolving picture of this complex process includes the following stages: irreversible or reversible adsorption, followed by denaturation and surface diffusion leading to eventual stabilization of the protein adlayer.[4,10–13] Aided by increasingly sophisticated macroscopic and microscopic measurements, there is growing acknowledgment of the fact that the behavior of adsorbing proteins can vary significantly at different surface coverages, in part reflecting the increasingly important role of protein–protein interactions at higher coverages.[14–17] Furthermore, numerous factors influence the adsorption process, including protein characteristics (*e.g.*, size, conformation, charge distribution),[18–23] substrate properties (*e.g.*, topography, atomic composition, surface charge),[24–28] and environmental conditions (*e.g.*, ionic strength, solution pH, temperature).[29–33] From a general perspective, ions are known to play an important role in modulating the interactions between proteins and solid supports.

[a] *School of Materials Science and Engineering, Nanyang Technological University, 50 Nanyang Avenue 639798, Singapore. E-mail: njcho@ntu.edu.sg*
[b] *Centre for Biomimetic Sensor Science, Nanyang Technological University, 50 Nanyang Drive 637553, Singapore*
[c] *School of Chemical and Biomedical Engineering, Nanyang Technological University, 62 Nanyang Drive 637459, Singapore*
† These authors contributed equally to this work.

While the influence of ionic strength on protein adsorption has been studied for several protein–surface models,[22,34–38] its broad spectrum of effects on protein structure, substrate chemistry, and the corresponding behavior of adsorbed proteins at solid–liquid interfaces motivates its further exploration because every case is unique to the specific conditions of the system under investigation, and application strategies inspired by ionic strength-dependent protein adsorption remain unexplored. In general, ionic strength can affect adsorption rate and total uptake by influencing protein–protein and protein–surface electrostatic interactions *via* charge-shielding effects[35–37] as well as direct binding of salt ions to the protein surface.[39–42] It has been noted that increased adsorption is observed when repulsive electrostatic interactions are effectively screened.[4] Intuitively, the trend in adsorption uptake with respect to ionic strength depends strongly on the overall net charge of the protein as well as the charge distribution. At the same time, the effects of ionic strength are nuanced and arguments strictly based on charge-shielding are sometimes insufficient to explain the observed trends in experimental data.

In one classical example, Ramsden and Prenosil reported that the adsorption rate and total uptake of apotransferrin (isoelectric point of 6.1) onto a negatively charged $Si(Ti)O_2$ surface decreased appreciably with increasing ionic strength.[34] This finding was intriguing because, under the experimental conditions, both the protein and the surface had negative net charges and it would be intuitively expected that increasing ionic strength promotes increased adsorption due to charge shielding. In order to investigate this issue, a rigorous quantitative approach was taken that showed that the surface coverage per adsorbed protein increased with increasing ionic strength arising from a corresponding increase in the net charge of the protein that causes interparticle repulsion as well as slower diffusion of protein molecules to the surface. As a result of the greater surface coverage per protein, the total protein uptake decreased at higher ionic strengths. While this study[34] outlined quantitative formulations to analyze protein adsorption at a general level, it was also noted that the theoretical calculations predicted an optimal salt concentration at which the surface coverage per protein molecule should be maximum, but a monotonic increase with increasing ionic strength was instead observed, leading the authors to suggest that salting-out effects may have induced the formation of some protein oligomers and highlighting the possible role of protein aggregation in influencing the adsorption kinetics. Collectively, all these findings point to the importance of empirical measurements for deciphering how ionic strength influences the adsorption of different types of proteins.

In this regard, one of the most abundant natural proteins, bovine serum albumin (BSA), is widely employed as a model for adsorption studies[43–52] and it is also one of the most common agents for surface passivation in molecular biology applications.[53–55] It is a relatively large globular protein (66.5 kDa) and negatively charged at physiological pH (isoelectric point of 4.7).[56] Despite its prevalence, the general effects of electrostatic interactions on the adsorption kinetics of BSA have so far been witnessed mostly through studies involving pH variation;[44,52] there is no consensus on incubation conditions (*e.g.*, protein concentration, salt concentration) that give the best passivation performance.[53,57–59] The effect of ionic strength on BSA adsorption remains an unanswered question in many respects. Several previous works have shown inconsistent trends in protein adsorption with respect to changes in ionic strength,[29,60–67] some of which appear counterintuitive if explanations based on electrostatic charge shielding are directly applied.[61–63] In certain cases, deviations from the expected trend have been attributed to salt ion accumulation around the protein affecting its conformational stability.[60,62,63] Using single-molecule analytical tools, McUmber *et al.* recently reported that the adsorption rate of individual BSA proteins onto silica surfaces strongly depends on the pH and ionic strength.[50] Under physiological pH conditions, the adsorption rate of individual proteins was greater at higher ionic strength, while non-electrostatic interactions were suggested to dominate the protein–surface interaction once adsorbed. Altogether, such studies at the single-molecule level motivate a number of promising directions to explore in the context of adsorbed BSA layers at saturation coverages, both in terms of fundamental understanding of protein–substrate and protein–protein interactions as well as practical application for preparing well-coated BSA layers for passivation applications.

The goal of the present study is to systematically investigate the effect of ionic strength on the adsorption behavior of BSA protein on silica. To approach this issue, we considered the effects of ionic strength on BSA protein stability and aggregation in solution as well as on protein adsorption, including the corresponding uptake and spreading of adsorbed proteins. Dynamic light scattering (DLS) and nanoparticle tracking analysis (NTA) were employed in order to measure the temporal onset of protein aggregation and the size range of protein aggregates over time along with circular dichroism (CD) spectroscopy experiments to investigate the protein secondary structure. Quartz crystal microbalance-dissipation (QCM-D) experiments were also conducted in order to measure the protein adsorption kinetics and uptake for BSA adsorption onto silica surfaces. Considering the general importance of BSA for passivation applications, we explored these aims in the context of both storage time before the experiment (*i.e.*, aggregation is a kinetically dependent process[68,69]), and the capability to prepare well-coated protein adlayers that could prevent nonspecific adsorption of serum onto the silica substrate.

## Materials and methods

### Sample preparation

Lyophilized bovine serum albumin (A2153) and sodium chloride (S7653, BioXtra) were obtained from Sigma-Aldrich (St. Louis, MO). The BSA was dissolved in the appropriate buffer solution and the final concentration of all BSA stock solutions was 50 μM, as determined by UV absorbance measurements at 280 nm. The buffer solutions contained 10 mM tris(hydroxymethyl)aminomethane (Tris) and the NaCl concentration was varied between 0 and 250 mM in 50 mM increments. The solution pH was

adjusted to 7.5. The freshly prepared BSA samples were stored at 4 °C until use.

### Dynamic light scattering

The effect of ionic strength on the size distribution of BSA protein molecules was investigated by using the DLS technique. A NanoBrook 90Plus particle size analyzer (Brookhaven Instruments, Holtsville, NY) was employed in order to measure the average size and size distribution of BSA molecules in the protein sample. All measurements were performed with a 658.0 nm monochromatic laser and recorded at a scattering angle of 90° in order to minimize the reflection effect. The intensity-weighted size distributions of the BSA molecules were recorded every day for up to one month, and the average diameter and standard deviation of protein samples are reported from $n$ = 5 measurements.

### Nanoparticle tracking analysis

A NanoSight LM10 instrument (Malvern Instruments, Malvern, UK) was employed to investigate the size distribution of protein aggregates in solution. The nanoparticle tracking analysis (NTA) was performed with a 405 nm laser and the transmitted light was recorded by a built-in sCMOS camera. Dilute protein samples were introduced into the sample chamber manually with a sterile disposable syringe until the solution reached the tip of the nozzle. All measurements were performed at room temperature and under ambient conditions. The laser beam experienced Rayleigh scattering when incident with the protein molecules and the scattered light from each protein molecule was visualized by optical microscope (20× magnification) and recorded by the sCMOS camera for a time period of 3 min at a rate of 25 frames per second. The measurement process was monitored and analyzed using the NTA 3.1 Build 3.1.46 software package. The hydrodynamic diameter of the protein molecules was calculated using the Stokes–Einstein equation from the time-resolved Brownian motion of individual particles tracked by the camera.

### Circular dichroism spectroscopy

CD spectra of the protein solution (50 μM BSA) were measured using an AVIV Model 420 spectrometer (AVIV Biomedical, Lakewood, NJ, USA) with a quartz cuvette that has a 1 mm path length. The background spectra were also measured in equivalent Tris buffer solution and then subtracted from the sample spectra. The CD spectra were recorded at room temperature of 24 °C across the spectral range of 190 to 260 nm in 0.5 nm intervals with a 4 s averaging time and 1.0 nm bandwidth. Each measurement was performed in triplicate. The ellipticity, expressed in units of millidegrees, was converted to the Molar Residue Ellipticity (MRE) by the following equation:

$$[\theta]\left(\text{degree cm}^2\ \text{dmol}^{-1}\right) = \frac{\text{millidegrees}}{n \times c \times l \times 10} \quad (1)$$

where $n$ represents the number of amino acid residues, $c$ is the protein concentration, and $l$ is the path length of the cuvette. The MRE at 222 nm was used to calculate the α-helicity of BSA protein by using the following equation:[70]

$$\text{helicity}(\%) = \frac{[\theta]_{222} - 3000}{-36000 - 3000} \times 100 \quad (2)$$

### Quartz crystal microbalance-dissipation (QCM-D)

A Q-Sense E4 instrument (Biolin Scientific, Stockholm, Sweden) was utilized to monitor BSA adsorption on silica-coated sensor chips (QSX303, Biolin Scientific). The surface of the sensor was cleaned by sequential rinsing with Milli-Q-treated water and ethanol, followed by drying with a stream of nitrogen gas. The surface of the sensor chip was then pre-treated with oxygen plasma (PDC-002, Harrick Plasma, Ithaca, NY, USA) for 2 min immediately before the experiment. As a control, atomic force microscopy experiments indicated that oxygen plasma treatment had only a minor effect on the surface roughness, and the root-mean-square surface roughness was typically around 1.3 nm across a 5 × 5 μm$^2$ silica surface with or without oxygen plasma treatment. It is worthy to note that surface roughness is known to have a strong effect on protein adsorption for fibrinogen but its effect on the adsorption of more globular BSA is modest.[27] All solutions were introduced into the measurement chamber through tubing with a 0.76 mm inner diameter (Pharmed, Ismatec SA, Switzerland) by a peristaltic pump (ISM833C, Ismatec SA) that was operated at a nominal flow rate of 0.1 mL min$^{-1}$. The shifts in the QCM-D resonance frequency and energy dissipation signals were recorded at several different odd overtones as a function of time. Data collected at the fifth overtone (25 MHz) are reported. The Voigt–Voinova model analysis was conducted in the Q-Sense Dfind software program (Biolin Scientific AB) as previously described,[71] and the density of the protein adlayer was constrained to be 1200 kg m$^{-3}$ (see, *e.g.*, ref. 72 for similar approaches).

## Results and discussion

### Colloidal stability of BSA protein

It is important to study the effect of ionic strength on the colloidal stability of proteins in aqueous solution prior to adsorption because the formation of aggregates can potentially change the adsorption behavior.[73] For example, it was recently found that antibody aggregates bind more strongly to a resin surface than antibody monomers.[74] Here, the colloidal stability of BSA in solution was monitored by tracking the temporal evolution of the protein size distribution with dynamic light scattering (DLS) and nanoparticle tracking analysis (NTA). DLS is an ensemble-average measurement technique that can detect particles ranging in size from a few nanometers to several microns but accurate size determination is challenging for polydisperse samples due to the DLS technique's inherent bias towards large particles.[75] On the other hand, NTA tracks the scattering of individual particles in the range of 30 nm to 1000 nm, allowing it to accurately measure the size distribution of protein oligomers but not monomers.[76] Taken together, DLS and NTA provide complementary information for characterizing

 

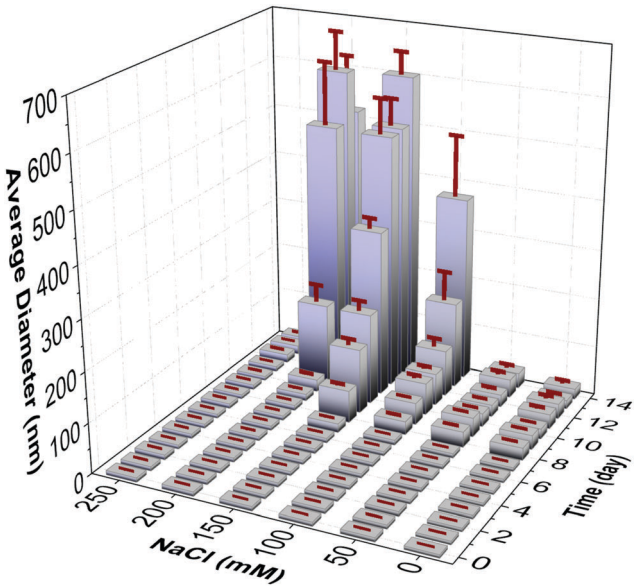


Fig. 1 DLS measurements of BSA protein size as a function of ionic strength and storage time. Time-dependent measurements of the average hydrodynamic diameter of BSA protein samples prepared in buffer solution with varying NaCl concentration are reported as mean ± standard deviation ($n$ = 5 measurements).

the size distribution of proteins in solution; DLS can detect both BSA protein monomers and oligomers, while NTA provides more accurate information about the size distribution of oligomers.

Immediately upon solubilization, the size distributions of BSA protein in aqueous solutions with different ionic strengths (0–250 mM NaCl) were measured using the DLS technique, as presented in Fig. 1. At this initial stage, it was observed that all samples exclusively contained protein monomers, with an average diameter of around 8 nm that agrees well with the expected value.[77] Additional DLS measurements were conducted periodically over a one-month storage period and it was concluded that the major fraction of protein molecules in solution is composed of protein monomers across the evaluated timespan. At the same time, some protein aggregation was also observed in a minor fraction and the kinetics of protein aggregation exhibited non-monotonic behavior with respect to increasing ionic strength. The kinetics of protein aggregation indicated that aggregation occurred more quickly in the range of 100 mM to 200 mM NaCl, whereas there was slower and less appreciable aggregation in higher or lower ionic strength conditions. After two weeks, measurements from DLS and NTA revealed the formation of distinct BSA populations with increasing ionic strength (Fig. 2), which is consistent with reported data on BSA fibrillation.[78] NTA also showed BSA aggregates becoming increasingly random in size with higher ionic strengths greater than 100 mM. One of the likely conjectures is that the distinct BSA populations are formed *via* different ("primary" and "secondary") mechanisms,[79,80] *e.g.*, the initial aggregate is driven by nucleation *via* reversible attachment of monomers, while the proceeding populations are subsequently formed *via* diffusion and coalescence.[80] With increasing ionic strength, effective charge screening not only occurs around protein monomers, but also around protein aggregates.[81,82] This allows aggregate–aggregate coalescence to occur to the same extent as monomer addition, adding diversity to the aggregate population. At the same time, the most pronounced protein aggregation occurred in the range of 100 to 200 mM NaCl and is attributed to the balance of salting-in and salting-out effects that influence protein aggregation due to the complex interplay of protein–ion and protein–protein interactions.[83] Overall, while some protein aggregation was observed, the main population of BSA molecules still consisted of monomers indicating that the initial oligomerization remains as the rate-limiting step regardless of the ionic strength.

Apart from establishing that most of the protein existed in monomeric form, we also investigated the secondary structure of BSA protein in solution, as presented in Fig. 3. Indeed, it is known that the binding of salt ions to the protein surface can affect conformational stability,[84–86] which is another important parameter governing protein adsorption.[20] Circular dichroism (CD) spectroscopy measurements were conducted and it was identified that there was no dependence of the BSA protein secondary structure on ionic strength. All the samples, including those that had been stored for up to one month, showed characteristic minima peaks at 208 and 222 nm, and a helical fraction of around 67%, which is in agreement with literature values[87] and confirms that the native α-helical character of BSA remained stable across the tested range of ionic strength conditions. This finding supports that the protein aggregation observed in our experiments likely arose from colloidal aggregation rather than extensive conformational changes. Indeed, for BSA, conformational changes in protein structure are typically indicated by changes in secondary structure.[88] In certain cases, secondary structure changes can occur while the overall steric conformation of the protein remains largely intact (see, *e.g.*, thermal denaturation[87]). On the basis of no changes being detected in secondary structure and the fact that the majority of BSA proteins remain in the monomeric state throughout the incubation period, the results support that the BSA molecules remain largely stable in the monomeric state across the different tested salt conditions.

### Protein adsorption onto silica surfaces

QCM-D experiments were next performed in order to investigate how ionic strength affects BSA protein adsorption onto a silica surface (Fig. 4). The QCM-D frequency and energy dissipation shifts were monitored as a function of time in order to characterize the mass and viscoelastic properties of the adlayer, respectively.[89] A baseline signal in aqueous buffer without protein was first established, and then 50 μM BSA protein in the equivalent buffer was added at $t$ = 7 min. A strong dependence on ionic strength was observed in the final frequency and dissipation shifts at adsorption saturation (Fig. 4a and b). At 0 mM NaCl salt concentration, the frequency shift reached around −72 Hz, whereas the frequency shift reached only −11 Hz at 250 mM NaCl salt concentration. There was a correlation between the ionic strength condition and maximum frequency shift across the full range of tested NaCl concentrations.

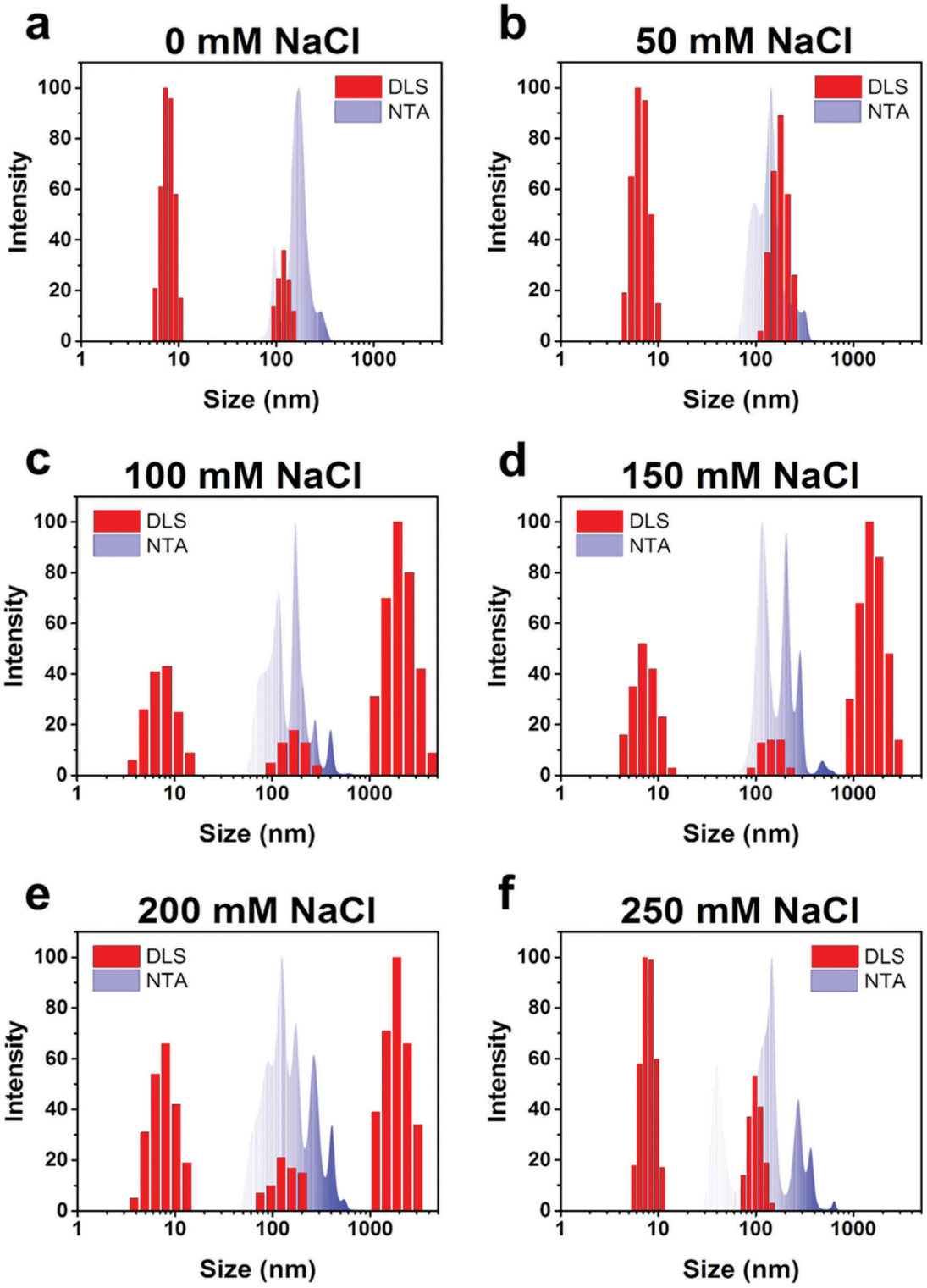


Fig. 2 DLS and NTA measurements of BSA protein size distribution after two weeks of storage in buffer solutions. Logarithmic scale representation of protein size distribution obtained from DLS (red; intensity-weighted) and NTA (blue; number-weighted) experiments. (a–f) Measurements were conducted for BSA protein samples in 10 mM Tris [pH 7.5] buffer solutions with varying NaCl salt concentrations.

Likewise, the energy dissipation shift reached around 4–6 $\times$ $10^{-6}$ in the low ionic strength regime (0–100 mM NaCl), whereas the energy dissipation shift reached $\sim$2.5 $\times$ $10^{-6}$ at 250 mM NaCl salt concentration, indicating that the adsorbed BSA layers are more rigidly attached to the silica surface at higher ionic strength. To analyze the adsorption process independently of time, the relationship between the energy dissipation shifts and frequency shifts for the different protein adsorption cases is presented in Fig. 4c.

 

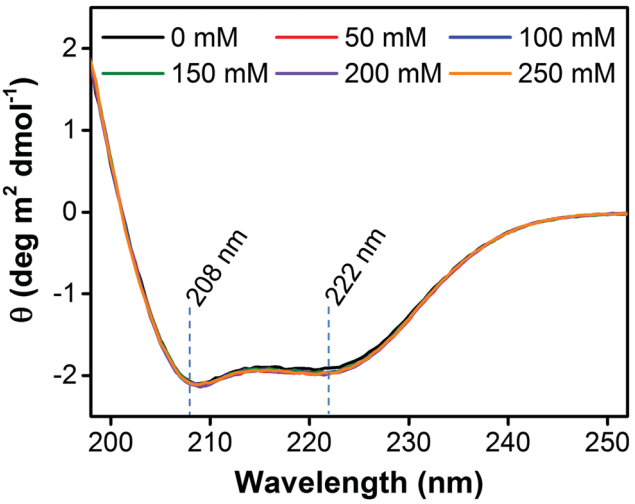


Fig. 3 Influence of ionic strength on BSA protein secondary structure. CD spectroscopy measurements were recorded in the UV spectral region (200–250 nm wavelength) in aqueous buffer solutions containing varying NaCl concentrations: 0 (black), 50 (red), 100 (blue), 150 (green), 200 (purple), and 250 mM (orange). Local minima at 208 nm and 222 nm are indicated and correspond to α-helical secondary structure characteristics.

The most unique behavior was seen in the 0 mM NaCl case, for which there was a positive slope that was observed until reaching a frequency shift of around −40 Hz and subsequent adsorption had only minor effects on the energy dissipation shift. In the higher surface coverage regime, this finding indicates that more adsorbed proteins had no additional effect on the viscoelastic properties of the adlayer and the generally complex behavior of the resulting frequency–dissipation curve suggests that protein adsorption in the absence of NaCl salt follows a modestly different pathway. By contrast, in the presence of NaCl salt, the initial slope of the frequency–dissipation curve was generally similar at all tested ionic strength conditions and a moderate decrease in the slope was observed at higher coverage regimes. For 150 mM NaCl and higher ionic strength conditions, a particularly noteworthy feature in the plots was evidence of a structural transformation at higher coverages, as indicated by a more significant change in the slope that suggested partial dehydration of the adsorbed protein layer.[90] The same series of experiments was conducted several times over the course of the BSA protein storage time in order to see if the minor protein aggregation affected the adsorption kinetics. As expected, a similar adsorption behavior was observed after various time durations of protein storage, which further supports that ionic strength is a governing parameter to modulate protein adsorption and that the effect of protein aggregation is nearly negligible in this system as the majority of molecules remain as monomers, as discussed above (Fig. 4d). Indeed, as protein adsorption is diffusion-limited and the diffusion coefficient of protein monomers in solution is much faster than that of protein oligomers,[10] it is reasonable to expect that the adsorbed protein layer would consist primarily of adsorbed monomers, at least before surface-induced reconfiguration. Taken together, the QCM-D data support that BSA adsorption uptake decreases with increasing ionic strength, especially in the range of 50 to 250 mM NaCl.

Based on this observed measurement trend, we analyzed the QCM-D data by using the Voigt–Voinova viscoelastic model to determine the effective thickness of the protein adlayer.[91] At 0 mM NaCl, the effective thickness of the bound BSA protein molecules was 12.7 nm, which is consistent with an end-on orientation of the molecules.[92] With increasing ionic strength, the effective thickness decreased to ∼4 nm in 200 to 250 mM NaCl conditions. This finding directly supports that the footprint of each bound protein molecule becomes larger with increasing ionic strength and is consistent with lower total uptake at higher ionic strengths. The variation in surface area per bound protein molecule could arise from the orientation of bound proteins and/or related differences in substrate-induced conformational changes. In either case, the QCM-D measurements and viscoelastic modeling provide direct evidence that there is greater protein spreading at higher ionic strengths. In order to explain this finding, we recall that silica surfaces are negatively charged under the experimental conditions while BSA molecules have a net negative charge as well. In the system, electrostatic repulsion would be expected and the extent of this repulsion would decrease at higher ionic strengths due to charge-shielding, in turn increasing the net strength of the protein–substrate interaction. Our observations agree well with this prediction and the related analytical model first described by Ramsden and Prenosil as discussed in the Introduction.[34] In particular, the smaller adlayer thicknesses observed for saturated BSA adlayers at higher ionic strength conditions support that there is greater protein spreading per molecule and this modeling result is also consistent with the recorded energy dissipation shifts, which indicate there are more rigidly attached protein adlayers at higher ionic strengths. Indeed, this behavior is consistent with greater protein spreading, which involves protein denaturation that includes partial dehydration,[11] as the concomitant increase in film rigidity is related to the QCM-D measurement technique's high sensitivity to hydrodynamically-coupled solvent. While such variations have been scrutinized in depth for adsorbed vesicles in the context of shape deformation, the general convention for QCM-D protein adsorption measurements is to associate greater/stronger adsorption with larger frequency shifts.[25,93]

Based on our experimental insights, the total uptake of adsorbed protein molecules (defined as adsorption) does increase with greater frequency shifts, but it is inversely related to the strength of the protein–substrate interaction. When the strength of the attractive interaction between adsorbed proteins and the substrate is relatively weak, the surface area per adsorbed protein molecule is comparatively small because each adsorbed protein is less spread out, resulting in a larger number of bound protein molecules per surface area (Fig. 4e). On the other hand, when the protein–substrate interaction is stronger, there is greater spreading of adsorbed proteins that in turn decreases the total number of bound protein molecules per surface area. Importantly, our experimental observations for BSA adsorption at saturation coverage are fully consistent with

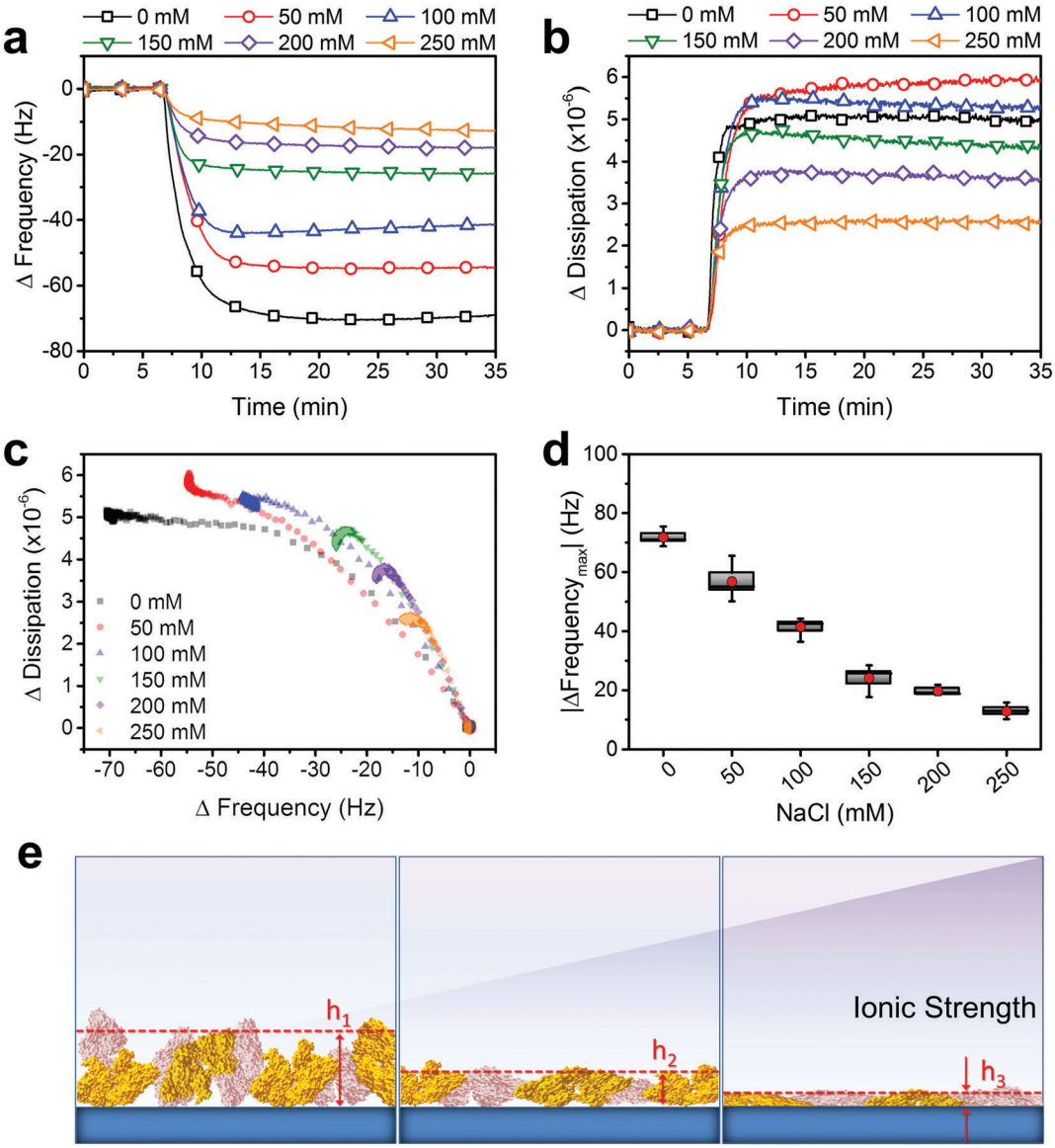


Fig. 4 QCM-D measurement of BSA protein adsorption onto silica surfaces as a function of ionic strength. Changes in (a) resonance frequency and (b) energy dissipation are reported as a function of time. The baseline was recorded in equivalent buffer solution and protein was added under continuous flow conditions from $t$ = 7 min onwards. The different NaCl concentrations are represented by: 0 (black), 50 (red), 100 (blue), 150 (green), 200 (purple), and 250 mM (orange). (c) Time-independent plot of energy dissipation shift as a function of resonance frequency shift for data from panels (a) and (b). (d) Descriptive statistics of maximum frequency shift values for protein adsorption under different NaCl conditions, as expressed by mean value (red dot) and standard deviation ($n$ = 6 measurements) within the rectangular columns along with the minimum and maximum measurement values (error bars). (e) Schematic illustration of protein adsorption onto a silica surface as a function of increasing ionic strength. At higher ionic strength conditions, protein spreading becomes more appreciable and the effective height ($h$) of the protein adlayer decreases, as measured by the QCM-D measurement technique.

recent single-molecule experiments indicating that there are more attractive interactions between BSA proteins and a silica surface at higher ionic strengths.[50] Hence, in our experiments, we observe that the total uptake of adsorbed protein molecules decreases with increasing ionic strength on account of stronger protein–substrate interactions and greater protein spreading.

### Desorption of BSA protein

In addition to protein adsorption, the effect of buffer rinsing on the stability of the protein adlayer formed was also investigated (Fig. 5). After the maximum uptake of adsorbed protein was reached, QCM-D measurements were continued and the protein solution in the measurement chamber was exchanged with the equivalent buffer solution (without protein). For comparison, the amount of protein desorption is normalized by the maximum frequency shift at saturation. In all cases, partial desorption of protein was observed (Fig. 5a). At 50 mM or greater NaCl salt concentration, there was approximately 30% or more removal of the adsorbed protein. By contrast, there was much less removal of protein adsorbed at 0 mM NaCl concentration, suggesting that adsorbed BSA molecules in the 0 mM NaCl condition were more tightly bound due to steric packing.[94–96] Indeed, the

 

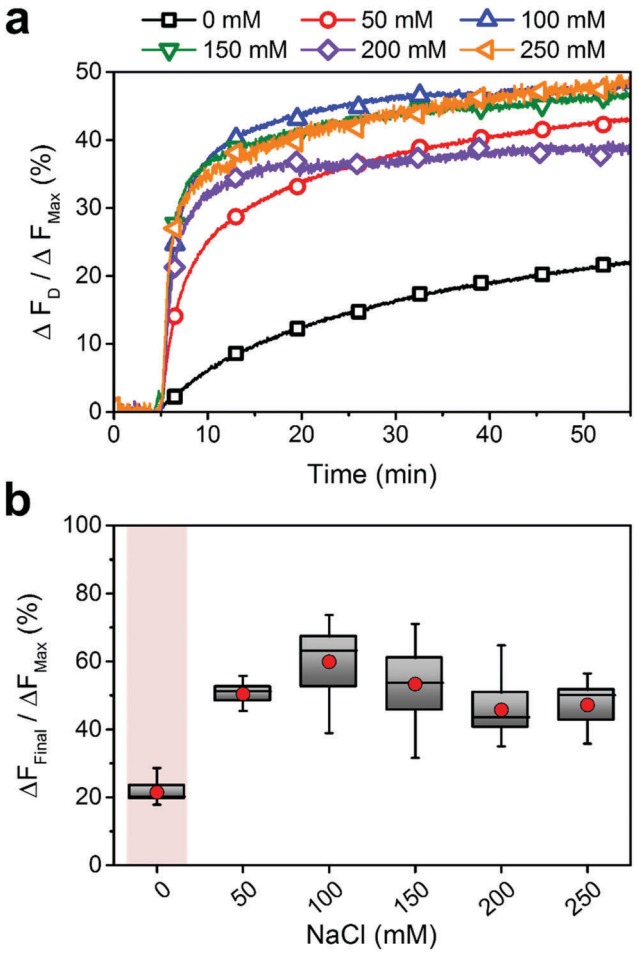


Fig. 5 QCM-D evaluation of protein desorption from an adsorbed BSA layer upon buffer rinsing. (a) Changes in resonance frequency are reported as a function of time. The baseline corresponds to the frequency shift associated with an adsorbed BSA layer at the appropriate ionic strength (normalized such that $\Delta F_{max}$ = 0 Hz at $t$ = 0 min). $\Delta F_D$ corresponds to the frequency shift associated with protein desorption upon buffer rinsing and this step is normalized by $\Delta F_{max}$ in order to calculate the % protein removal for comparison across the different cases. Protein desorption began with a buffer rinsing step that was performed under continuous flow conditions from $t$ = 5 min onwards. The different NaCl conditions are represented by: 0 (black), 50 (red), 100 (blue), 150 (green), 200 (purple), and 250 mM (orange). (b) Descriptive statistics of maximum frequency shift measurements, as expressed by mean value (red dot) and standard deviation ($n$ = 6 measurements) within the rectangular columns along with the minimum and maximum measurement values (error bars).

fraction of desorbed BSA protein at 50 mM or greater NaCl salt concentrations was statistically equivalent across this ionic strength range and supports that some weakly bound protein was removed in order to promote more favorable interactions among the remaining bound proteins (*e.g.*, greater spreading on the surface)[97] (Fig. 5b). Taken together, the findings indicate that the largest uptake of bound protein was recorded in buffer solution without NaCl salt. It also reinforces the notion that BSA protein adsorption on silica follows different pathways depending on the presence of NaCl salt, with the specific ionic strength of the solution further controlling the extent of protein spreading.

### Utility for surface passivation

BSA is widely used as a blocking agent to coat surfaces in order to prevent nonspecific adsorption and fouling.[98] As mentioned in the Introduction, the optimal conditions for BSA deposition on a substrate are not fully clear and BSA solutions are commonly prepared in deionized water or in aqueous buffers with varying salt concentrations. Based on the observed high uptake of adsorbed BSA in the absence of NaCl salt, we hypothesized that pretreatment of a silica surface with adsorbed BSA layers under this condition would confer high surface passivation against serum fouling. In order to test this hypothesis, we employed the QCM-D measurement technique to measure the blocking efficiency of adsorbed BSA films against surface fouling upon incubation with whole fetal bovine serum (FBS), which is a mixture of diverse proteins and other biological components.[99] Representative QCM-D responses are presented in Fig. 6a and show the detailed steps involved in the surface passivation experiments. After establishing a baseline signal in Tris buffer with 150 mM NaCl salt concentration, the buffer was exchanged to Tris buffer with the appropriate NaCl salt concentration, either containing 0 or 150 mM NaCl. Then, 50 μM BSA protein in the equivalent buffer was added, leading to −71 and −15 Hz frequency shifts for BSA adsorption in 0 and 150 mM NaCl salt concentrations, respectively (Fig. 6a, step i). A rinsing step with Tris buffer with 150 mM NaCl solution was next applied in order to remove weakly bound protein and also roughly mimic the ionic strength of FBS (Fig. 6a, step ii). For the case of protein adsorption at 0 mM NaCl, approximately 90% of adsorbed BSA was removed, while for the case of 150 mM NaCl, about 60% protein removal was observed. The 0 mM NaCl case is particularly noteworthy because it supports that the no-salt condition is important for maintaining large uptake, and the adsorbed BSA at 0 mM NaCl is largely removed when the buffer condition is exchanged to 150 mM NaCl salt concentration. This agrees well with expectations because the protein–substrate interaction is more attractive under higher ionic salt conditions, and hence greater protein spreading will lead to removal of some bound proteins due to the larger surface area per bound protein molecule. Next, 100% FBS was injected causing a large negative shift in the frequency signal due to a combination of fouling and differences in the bulk solution properties[100] (Fig. 6a, step iii). The bulk solution was then exchanged back to Tris buffer with 150 mM NaCl, and the frequency shift attributed to FBS elements that caused surface fouling was determined by subtracting the frequency shift of the adsorbed BSA layer in 150 mM NaCl (defined as the value after step ii was completed) from the final frequency shift (Fig. 6a, step iv). The corresponding frequency shifts were −53 and −50 Hz for adsorbed BSA layers formed under 0 and 150 mM NaCl salt concentrations, respectively. In order to determine the passivation efficiency, a control experiment was run on a bare silica substrate without BSA coating and the corresponding frequency shift in this case (−65 Hz) served as the reference value for 0% blocking. Based on these values, it was determined that the adsorbed BSA layers formed under 0 mM and 150 mM NaCl salt concentrations demonstrated 18 and 23% blocking efficiency, respectively.

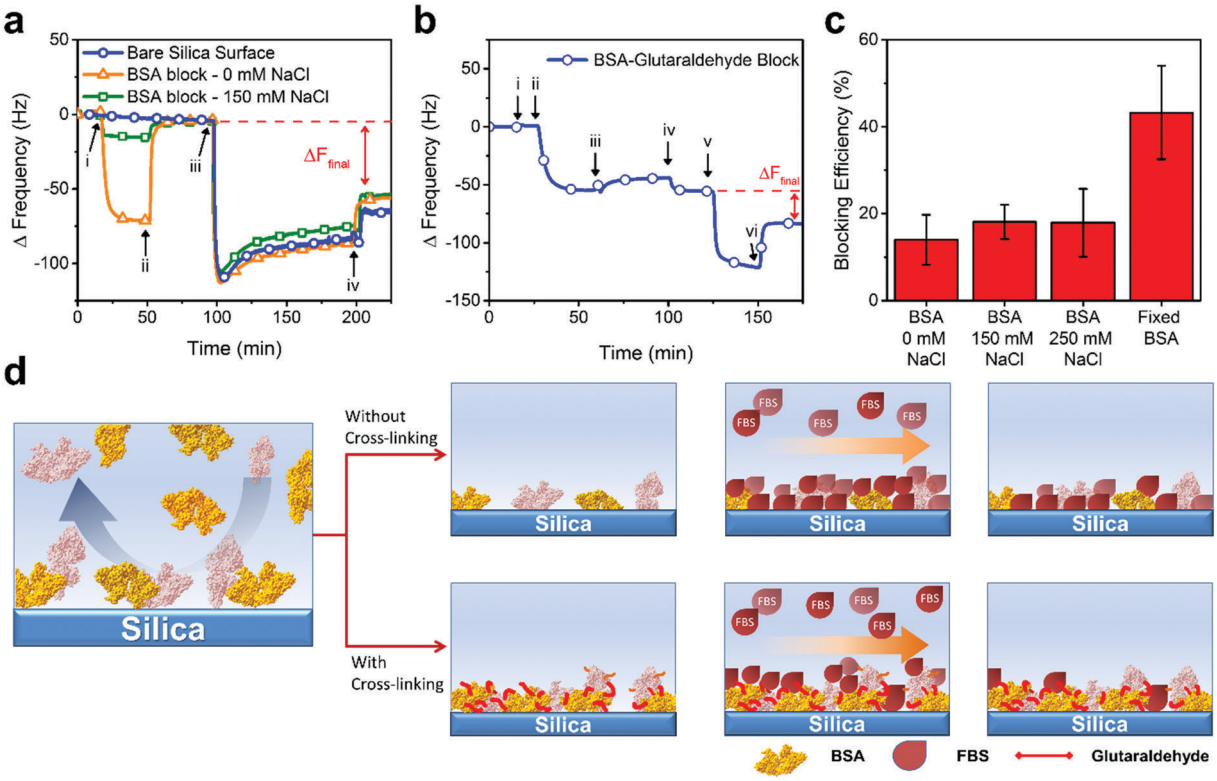


Fig. 6 QCM-D evaluation of BSA protein blocking performance against fetal bovine serum (FBS) fouling on silica surfaces. (a) Changes in resonance frequency are reported as a function of time. The baseline was recorded in Tris buffer with 150 mM NaCl and then exchanged to the appropriate NaCl concentration before the following steps: (i) 50 μM BSA addition in Tris buffer with the appropriate NaCl concentration, (ii) buffer rinse with Tris buffer with 150 mM NaCl, (iii) 100% FBS injection, and (iv) buffer rinse with Tris buffer solution with 150 mM NaCl. BSA deposition in 0 and 150 mM NaCl is indicated by orange triangles and green squares, respectively. A control experiment without BSA coating was run on a bare silica surface and is indicated by blue circles. Note that a similar experiment with 50 μM BSA deposition in 250 mM NaCl was also conducted and the results are reported in panel (c). (b) Changes in resonance frequency are reported as a function of time. The baseline was recorded in Tris buffer with 150 mM NaCl followed by: (i) exchange to Tris buffer with 0 mM NaCl, (ii) 50 μM BSA addition in Tris buffer with 0 mM NaCl, (iii) treatment with 0.1% gluteraldehyde in Tris buffer with 0 mM NaCl, (iv) buffer rinse with Tris buffer solution with 150 mM NaCl, (v) 100% FBS injection, and (vi) buffer rinse with Tris buffer solution with 150 mM NaCl. (c) Calculated blocking efficiency of adsorbed BSA protein layers prepared under different NaCl concentrations or cross-linked BSA prepared from deposited BSA in 0 mM NaCl. Data are expressed as mean ± standard deviation ($n$ = 3 measurements). (d) Schematic illustration of adsorbed BSA passivation layers without or with gluteraldehyde cross-linking.

To take advantage of high protein uptake under the 0 mM NaCl condition, we therefore decided to introduce a subsequent gluteraldehyde cross-linking step in order to stabilize the adsorbed BSA. Indeed, gluteraldheyde and related fixation agents enable covalent cross-linking of adsorbed protein molecules.[101–103] A representative QCM-D response detailing the modified protocol is presented in Fig. 6b. The baseline was first established in Tris buffer with 150 mM NaCl before exchange with Tris buffer with 0 mM NaCl (Fig. 6b, step i). Then, 50 μM BSA in 0 mM NaCl was added to the silica surface followed by incubation with 0.1% glutaraldehyde in an equivalent buffer solution (Fig. 6b, steps ii–iii). The gluteraldehye cross-linking step led to an increase in the frequency shift from approximately −56 Hz to −43 Hz, which is characteristic of the adsorbed protein film becoming more rigid.[104,105] Afterwards, the solvent was exchanged to Tris buffer with 150 mM NaCl (Fig. 6b, step iv) which returned a negative frequency shift. Importantly, in marked contrast to the case without covalent cross-linking, the frequency shift in 150 mM was around −55 Hz, which supported that cross-linking stabilizes the adsorbed BSA molecules. 100% FBS was then added followed by a subsequent buffer wash with Tris buffer with 150 mM NaCl and the final frequency shift attributed to FBS fouling was −28 Hz, which corresponds to 57% blocking efficiency (Fig. 6b, steps v–vi).

As such, the findings indicate that controlling the adsorption uptake of BSA protein onto silica surfaces is insufficient by itself to improve passivation efficiency because the bound proteins molecules likely undergo conformational changes in response to variations in ionic strength and corresponding changes in the strength of the protein–substrate interaction. As a result, the passivation efficiency is around 15–20% in all cases (Fig. 6c). On the other hand, gluteraldehyde cross-linking significantly improves the passivation efficiency by two-to-three fold because it stabilizes bound protein against ionic strength variations. The subsequent cross-linking step allows one to take advantage of specific protocols that improve BSA uptake such as using low ionic strength conditions, as schematically illustrated in Fig. 6d. Altogether, understanding how ionic strength affects BSA protein

 

adsorption onto silica surfaces not only sheds light on the fundamental interactions underpinning BSA protein–substrate interactions but also offers a practical method to improve surface passivation strategies.

## Conclusion

In summary, we have systematically investigated how ionic strength affects the solution properties and adsorption behavior of BSA protein, and utilized this knowledge to establish an improved protein-based surface passivation strategy on silica surfaces. In particular, we discovered that ionic strength had only modest effects on the aggregation properties of protein molecules in solution, whereas it had a striking effect on the adsorption behavior of protein molecules onto silica surfaces and strongly influenced the degree of protein spreading, as reflected in the total protein uptake at saturation and corresponding viscoelastic modeling of the adlayer's effective thickness. In this regard, a key innovative aspect of our findings was that ionic strength modulation of protein adsorption was further aided by covalent cross-linking in order to stabilize protein molecules that were initially adsorbed under low ionic strength conditions. The covalent cross-linking provided a structural reinforcement that made the protein adlayer largely impervious to subsequent ionic strength modulation (*e.g.*, solvent-exchange to higher ionic strength conditions) and hence the bound protein molecules remained stable under physiologically relevant ionic strength conditions. As a result, the cross-linked BSA protein molecules that were deposited under low ionic strength conditions offered a marked improvement in surface passivation against serum fouling on the silica surface *via* pronounced steric blocking. Taken together, the findings in this work not only improve our understanding of how ionic strength influences BSA protein adsorption onto solid supports but also provide guidance on how ionic strength conditions can be utilized for developing improved surface passivation strategies. Moreover, as BSA was found to be highly stable in aqueous solutions over long periods of time, its utility as a blocking agent is further reinforced and the role of ionic strength in improving surface passivation deserves attention across a wider range of hydrophobic and hydrophilic substrates in general.

## Acknowledgements

This work was supported by a National Research Foundation Proof-of-Concept Grant (NRF2015NRF-POC001-019). The authors thank V. P. Zhdanov for valuable discussions and suggestions on the manuscript and E. Linardy for technical assistance with experiments.

## References

1 M. Malmsten, *Biopolymers at Interfaces*, CRC Press, 2nd edn, 2003.
2 J. J. Gray, *Curr. Opin. Struct. Biol.*, 2004, **14**, 110–115.
3 T. S. Tsapikouni and Y. F. Missirlis, *Mater. Sci. Eng., B*, 2008, **152**, 2–7.
4 M. Rabe, D. Verdes and S. Seeger, *Adv. Colloid Interface Sci.*, 2011, **162**, 87–106.
5 A. Garland, L. Shen and X. Zhu, *Prog. Surf. Sci.*, 2012, **87**, 1–22.
6 M. P. Monopoli, C. Aberg, A. Salvati and K. A. Dawson, *Nat. Nanotechnol.*, 2012, **7**, 779–786.
7 M. Kastantin, B. B. Langdon and D. K. Schwartz, *Adv. Colloid Interface Sci.*, 2014, **207**, 240–252.
8 A. S. Timin, A. V. Solomonov, I. I. Musabirov, S. N. Sergeev, S. P. Ivanov, E. V. Rumyantsev and A. Goncharenko, *Ind. Eng. Chem. Res.*, 2014, **53**, 13699–13710.
9 A. Timin, E. Rumyantsev and A. Solomonov, *J. Non-Cryst. Solids*, 2014, **385**, 81–88.
10 V. P. Zhdanov and B. Kasemo, *Surf. Rev. Lett.*, 1998, **05**, 615–634.
11 E. A. Vogler, *Biomaterials*, 2012, **33**, 1201–1237.
12 F. Y. Yohko, *J. Phys.: Condens. Matter*, 2012, **24**, 503101.
13 L. Yu, L. Zhang and Y. Sun, *J. Chromatogr. A*, 2015, **1382**, 118–134.
14 M. Chen, T. Zheng, C. Wu and C. Xing, *Colloids Surf., B*, 2014, **121**, 150–157.
15 F. De Leo, A. Magistrato and D. Bonifazi, *Chem. Soc. Rev.*, 2015, **44**, 6916–6953.
16 M. Panos, T. Z. Sen and M. G. Ahunbay, *Langmuir*, 2012, **28**, 12619–12628.
17 G. Raffaini and F. Ganazzoli, *Langmuir*, 2010, **26**, 5679–5689.
18 W. Norde and A. C. I. Anusiem, *Colloids Surf.*, 1992, **66**, 73–80.
19 F. Fang and I. Szleifer, *J. Chem. Phys.*, 2003, **119**, 1053–1065.
20 M. Karlsson, J. Ekeroth, H. Elwing and U. Carlsson, *J. Biol. Chem.*, 2005, **280**, 25558–25564.
21 P. Roach, D. Farrar and C. C. Perry, *J. Am. Chem. Soc.*, 2005, **127**, 8168–8173.
22 T. S. Tsapikouni and Y. F. Missirlis, *Colloids Surf., B*, 2007, **57**, 89–96.
23 M. M. Ouberai, K. Xu and M. E. Welland, *Biomaterials*, 2014, **35**, 6157–6163.
24 M. P. Calatayud, B. Sanz, V. Raffa, C. Riggio, M. R. Ibarra and G. F. Goya, *Biomaterials*, 2014, **35**, 6389–6399.
25 A. Dolatshahi-Pirouz, K. Rechendorff, M. B. Hovgaard, M. Foss, J. Chevallier and F. Besenbacher, *Colloids Surf., B*, 2008, **66**, 53–59.
26 S. Pasche, J. Vörös, H. J. Griesser, N. D. Spencer and M. Textor, *J. Phys. Chem. B*, 2005, **109**, 17545–17552.
27 K. Rechendorff, M. B. Hovgaard, M. Foss, V. P. Zhdanov and F. Besenbacher, *Langmuir*, 2006, **22**, 10885–10888.
28 P. Roach, D. Farrar and C. C. Perry, *J. Am. Chem. Soc.*, 2006, **128**, 3939–3945.
29 K. L. Jones and C. R. O'Melia, *J. Membr. Sci.*, 2000, **165**, 31–46.
30 E. Seyrek, P. L. Dubin, C. Tribet and E. A. Gamble, *Biomacromolecules*, 2003, **4**, 273–282.

31 T. Kopac, K. Bozgeyik and J. Yener, *Colloids Surf., A*, 2008, **322**, 19–28.
32 H. Mo, K. G. Tay and H. Y. Ng, *J. Membr. Sci.*, 2008, **315**, 28–35.
33 T. Wei, S. Kaewtathip and K. Shing, *J. Phys. Chem. C*, 2009, **113**, 2053–2062.
34 J. J. Ramsden and J. E. Prenosil, *J. Phys. Chem.*, 1994, **98**, 5376–5381.
35 M. Lundin, U. M. Elofsson, E. Blomberg and M. W. Rutland, *Colloids Surf., B*, 2010, **77**, 1–11.
36 J. Mathes and W. Friess, *Eur. J. Pharm. Biopharm.*, 2011, **78**, 239–247.
37 A. Bratek-Skicki, P. Żeliszewska, Z. Adamczyk and M. Cieśla, *Langmuir*, 2013, **29**, 3700–3710.
38 L. Tercinier, A. Ye, A. Singh, S. G. Anema and H. Singh, *Food Biophys.*, 2014, **9**, 341–348.
39 P. R. Majhi, R. R. Ganta, R. P. Vanam, E. Seyrek, K. Giger and P. L. Dubin, *Langmuir*, 2006, **22**, 9150–9159.
40 J. Juárez, S. G. López, A. Cambón, P. Taboada and V. Mosquera, *J. Phys. Chem. B*, 2009, **113**, 10521–10529.
41 L. Ianeselli, F. Zhang, M. W. A. Skoda, R. M. J. Jacobs, R. A. Martin, S. Callow, S. Prévost and F. Schreiber, *J. Phys. Chem. B*, 2010, **114**, 3776–3783.
42 A. K. Buell, P. Hung, X. Salvatella, M. E. Welland, C. M. Dobson and T. P. J. Knowles, *Biophys. J.*, 2013, **104**, 1116–1126.
43 T. J. Su, J. R. Lu, R. K. Thomas, Z. F. Cui and J. Penfold, *J. Phys. Chem. B*, 1998, **102**, 8100–8108.
44 T. J. Su, J. R. Lu, R. K. Thomas and Z. F. Cui, *J. Phys. Chem. B*, 1999, **103**, 3727–3736.
45 C. E. Giacomelli and W. Norde, *J. Colloid Interface Sci.*, 2001, **233**, 234–240.
46 G. Jackler, R. Steitz and C. Czeslik, *Langmuir*, 2002, **18**, 6565–6570.
47 H. Larsericsdotter, S. Oscarsson and J. Buijs, *J. Colloid Interface Sci.*, 2005, **289**, 26–35.
48 K. M. Yeung, Z. J. Lu and N. H. Cheung, *Colloids Surf., B*, 2009, **69**, 246–250.
49 M. Wiśniewska, K. Szewczuk-Karpisz and D. Sternik, *J. Therm. Anal. Calorim.*, 2014, **120**, 1355–1364.
50 A. C. McUmber, T. W. Randolph and D. K. Schwartz, *J. Phys. Chem. Lett.*, 2015, **6**, 2583–2587.
51 J. Meissner, A. Prause, B. Bharti and G. H. Findenegg, *Colloid Polym. Sci.*, 2015, **293**, 3381–3391.
52 B. Jachimska, K. Tokarczyk, M. Łapczyńska, A. Puciul-Malinowska and S. Zapotoczny, *Colloids Surf., A*, 2016, **489**, 163–172.
53 M. Steinitz, *Anal. Biochem.*, 2000, **282**, 232–238.
54 B. Sweryda-Krawiec, H. Devaraj, G. Jacob and J. J. Hickman, *Langmuir*, 2004, **20**, 2054–2056.
55 E. I. Silva-López, L. E. Edens, A. O. Barden, D. J. Keller and J. A. Brozik, *Chem. Phys. Lipids*, 2014, **183**, 91–99.
56 C. B. Anfinsen, J. T. Edsall and F. M. Richards, *Adv. Protein Chem.*, Academic Press, 1976.
57 Y. Jeyachandran, J. Mielczarski, E. Mielczarski and B. Rai, *J. Colloid Interface Sci.*, 2010, **341**, 136–142.
58 Y. Xiao and S. N. Isaacs, *J. Immunol. Methods*, 2012, **384**, 148–151.
59 R. Ahirwar, S. Bariar, A. Balakrishnan and P. Nahar, *RSC Adv.*, 2015, **5**, 100077.
60 W. Norde and J. Lyklema, *J. Colloid Interface Sci.*, 1978, **66**, 257–265.
61 V. Hlady and H. Füredi-Milhofer, *J. Colloid Interface Sci.*, 1979, **69**, 460–468.
62 T. Suzawa, H. Shirahama and T. Fujimoto, *J. Colloid Interface Sci.*, 1982, **86**, 144–150.
63 H. Shirahama and T. Suzawa, *Colloid Polym. Sci.*, 1985, **263**, 141–146.
64 D. T. H. Wassell, R. C. Hall and G. Embery, *Biomaterials*, 1995, **16**, 697–702.
65 S. Fukuzaki, H. Urano and K. Nagata, *J. Ferment. Bioeng.*, 1996, **81**, 163–167.
66 S. Salgın, S. Takaç and T. H. Özdamar, *J. Membr. Sci.*, 2006, **278**, 251–260.
67 N. Shamim, L. Hong, K. Hidajat and M. S. Uddin, *J. Colloid Interface Sci.*, 2006, **304**, 1–8.
68 J. J. Babcock and L. Brancaleon, *Int. J. Biol. Macromol.*, 2013, **53**, 42–53.
69 M. Bhattacharya, N. Jain and S. Mukhopadhyay, *J. Phys. Chem. B*, 2011, **115**, 4195–4205.
70 N. Greenfield and G. D. Fasman, *Biochemistry*, 1969, **8**, 4108–4116.
71 M. V. Voinova, M. Rodahl, M. Jonson and B. Kasemo, *Phys. Scr.*, 1999, **59**, 391.
72 M. Lundin, Y. Hedberg, T. Jiang, G. Herting, X. Wang, E. Thormann, E. Blomberg and I. O. Wallinder, *J. Colloid Interface Sci.*, 2012, **366**, 155–164.
73 E. Y. Chi, S. Krishnan, T. W. Randolph and J. F. Carpenter, *Pharm. Res.*, 2003, **20**, 1325–1336.
74 D. Yu, Y. Song, R. Y.-C. Huang, R. K. Swanson, Z. Tan, E. Schutsky, A. Lewandowski, G. Chen and Z. J. Li, *J. Chromatogr. A*, 2016, **1457**, 66–75.
75 P. A. Hassan, S. Rana and G. Verma, *Langmuir*, 2014, **31**, 3–12.
76 V. Filipe, A. Hawe and W. Jiskoot, *Pharm. Res.*, 2010, **27**, 796–810.
77 S. Li, D. Xing and J. Li, *J. Biol. Phys.*, 2004, **30**, 313–324.
78 J. J. Babcock and L. Brancaleon, *Int. J. Biol. Macromol.*, 2013, **53**, 42–53.
79 T. Nicolai and D. Durand, *Curr. Opin. Colloid Interface Sci.*, 2013, **18**, 249–256.
80 C. J. Roberts, *Biotechnol. Bioeng.*, 2007, **98**, 927–938.
81 P. Aymard, T. Nicolai, D. Durand and A. Clark, *Macromolecules*, 1999, **32**, 2542–2552.
82 E. P. Schokker, H. Singh, D. N. Pinder and L. K. Creamer, *Int. Dairy J.*, 2000, **10**, 233–240.
83 H.-N. Xu, Y. Liu and L. Zhang, *Soft Matter*, 2015, **11**, 5926–5932.
84 C. Nishimura, V. N. Uversky and A. L. Fink, *Biochemistry*, 2001, **40**, 2113–2128.
85 D. Shukla, C. P. Schneider and B. L. Trout, *J. Am. Chem. Soc.*, 2011, **133**, 18713–18718.

 

86 R. Majumdar, P. Manikwar, J. M. Hickey, H. S. Samra, H. A. Sathish, S. M. Bishop, C. R. Middaugh, D. B. Volkin and D. D. Weis, *Biochemistry*, 2013, **52**, 3376–3389.
87 Y. Moriyama, E. Watanabe, K. Kobayashi, H. Harano, E. Inui and K. Takeda, *J. Phys. Chem. B*, 2008, **112**, 16585–16589.
88 T. Peters Jr, *All about albumin: biochemistry, genetics, and medical applications*, Academic Press, 1995.
89 N.-J. Cho, C. W. Frank, B. Kasemo and F. Höök, *Nat. Protoc.*, 2010, **5**, 1096–1106.
90 T. Q. Luong, P. K. Verma, R. K. Mitra and M. Havenith, *Biophys. J.*, 2011, **101**, 925–933.
91 M. Voinova, M. Jonson and B. Kasemo, *Biosens. Bioelectron.*, 2002, **17**, 835–841.
92 P. G. Squire, P. Moser and C. T. O'Konski, *Biochemistry*, 1968, **7**, 4261–4272.
93 A. A. Feiler, A. Sahlholm, T. Sandberg and K. D. Caldwell, *J. Colloid Interface Sci.*, 2007, **315**, 475–481.
94 A. P. Minton, *Biophys. Chem.*, 2000, **86**, 239–247.
95 A. P. Minton, *Biophys. J.*, 2001, **80**, 1641–1648.
96 G. Anand, S. Sharma, A. K. Dutta, S. K. Kumar and G. Belfort, *Langmuir*, 2010, **26**, 10803–10811.
97 V. Ball, A. Bentaleb, J. Hemmerle, J.-C. Voegel and P. Schaaf, *Langmuir*, 1996, **12**, 1614–1621.
98 J. Gibbs and M. Kennebunk, *ELISA Technical Bulletin*, Corning Incorporated Life Sciences, Kennebunk, ME, 2001.
99 K. V. Honn, J. A. Singley and W. Chavin, *Exp. Biol. Med.*, 1975, **149**, 344–347.
100 S. Bruckenstein and M. Shay, *Electrochim. Acta*, 1985, **30**, 1295–1300.
101 Y. An, G. Stuart, S. McDowell, S. McDaniel, Q. Kang and R. Friedman, *J. Orthop. Res.*, 1996, **14**, 846–849.
102 F. López-Gallego, L. Betancor, C. Mateo, A. Hidalgo, N. Alonso-Morales, G. Dellamora-Ortiz, J. M. Guisán and R. Fernández-Lafuente, *J. Biotechnol.*, 2005, **119**, 70–75.
103 S. J. Geelhood, T. A. Horbett, W. K. Ward, M. D. Wood and M. J. Quinn, *J. Biomed. Mater. Res., Part B*, 2007, **81**, 251–260.
104 C. Fant, K. Sott, H. Elwing and F. Hook, *Biofouling*, 2000, **16**, 119–132.
105 F. Höök, B. Kasemo, T. Nylander, C. Fant, K. Sott and H. Elwing, *Anal. Chem.*, 2001, **73**, 5796–5804.